ARTICLE
Journal of Cellular Biochemistry 106:570–579 (2009)

Journal of Cellular Biochemistry

Quantitative Proteomic Analysis of Differential Proteins in the Stroma of Nasopharyngeal Carcinoma and Normal Nasopharyngeal Epithelial Tissue

Mei-Xiang Li,[1,2,3] Zhi-Qiang Xiao,[1] Ying-Fu Liu,[1,2] Yong-Heng Chen,[4] Cui Li,[1] Peng-Fei Zhang,[1] Mao-Yu Li,[1] Feng Li,[2] Fang Peng,[1] Chao-Jun Duan,[1] Hong Yi,[1] Hui-Xin Yao,[1,2] and Zhu-Chu Chen[1,2*]

[1]*Key Laboratory of Cancer Proteomics of Chinese Ministry of Health, Xiangya Hospital, Central South University, Changsha 410008, Hunan Province, China*

[2]*Cancer Research Institute, Xiangya School of Medicine, Central South University, Changsha 410078, Hunan Province, China*

[3]*Department of Histology and Embryology, University of South China, Hengyang 421001, Hunan Province, China*

[4]*Molecular & Computational Biology, University of Southern California, Los Angeles, California*

ABSTRACT

The importance of stromal cells and the factors that they expressed during cancer initiation and progression have been highlighted by recent literature. To identify the stromal proteins involved in nasopharyngeal carcinoma (NPC) carcinogenesis, we assessed differences in protein expression of the stroma from NPC and normal nasopharyngeal epithelium tissues (NNET) using a quantitative proteomic approach combined with laser capture microdissection (LCM). LCM was performed to purify stromal cells from the NPC and NNET, respectively. The differential proteins between the pooled microdissected tumor and normal stroma were analyzed by two-dimensional difference gel electrophoresis (2D-DIGE) combined with mass spectrometry (MS). Twenty differential proteins were identified, and the expression and location of two differential proteins (L-plastin and S100A9) were further confirmed by Western blotting and immunohistochemical analysis. Our results will be helpful to study the role of stroma in the NPC carcinogenesis, as well as discover the interaction between NPC cells and their surrounding microenvironment. J. Cell. Biochem. 106: 570–579, 2009.

KEY WORDS: NASOPHARYNGEAL CARCINOMA; STROMA; LASER CAPTURE MICRODISSECTION; 2-D DIGE; CARCINOGENESIS

Carcinomas in general are composed of two interdependent components: the neoplastic epithelial cells and the supporting tumor stroma (TS). The latter plays an important role in pivotal processes such as tumor proliferation, vascularization, invasion, and metastasis [Wernert, 1997; Liotta and Kohn, 2001; Wernert et al., 2001]. Cancer cells, stromal cell compartment, and the extracellular matrix (ECM) generate a multifaceted tumor microenvironment [Cruz-Munoz et al., 2006]. The distinct molecular "cross-talk" between cancer cells and surrounding host cells is currently being examined in a number of settings [Liotta and Kohn, 2001]. Such signaling can result in modification of the microenvironment by the tumor cells themselves, in order to facilitate tumor invasion and progression. Host stromal cells may also influence tumor behavior [Muerkoster et al., 2004; Ohuchida et al., 2004] and stimulate tumor proliferation [Olumi et al., 1999]. In addition to influencing tumor behavior, specific stromal components have also emerged as markers of poor survival in cancer patients [Bingle et al., 2002; Koukourakis et al., 2003]. In recent years, there have been numerous reports demonstrating that growth and progression of tumor cells depend not only on their malignant potential but also on stromal

Grant sponsor: National Key Basic Research Program of China; Grant sponsor: Ministry of Education of China; Grant sponsor: Hibiscus Scholars of Hunan Province, China; Grant sponsor: Science and Technology Committee of Hunan, China; Grant sponsor: Public Health Bureau of Hunan Province, China; Grant sponsor: National Natural Sciences Foundation of China; Grant numbers: 2001CB510207, 2002-48, 2007-362, 04XK1001-1, 05SK1004-1, Z02-04, 30500558, 30670990, 2007-70.

*Correspondence to: Zhu-Chu Chen, Key Laboratory of Cancer Proteomics of Chinese Ministry of Health, Xiangya Hospital, Central South University, 87# Xiangya Road, Changsha 410008, Hunan, China. E-mail: tcbl@xysm.net

Received 25 August 2008; Accepted 20 November 2008 • DOI 10.1002/jcb.22028 • 2009 Wiley-Liss, Inc.
Published online 13 January 2009 in Wiley InterScience (www.interscience.wiley.com).

factors present in the tumor microenvironment, the insoluble ECM and cell–cell interactions [Coussens and Werb, 2001; Fidler, 2001; Liotta and Kohn, 2001; Silberstein, 2001; Wiseman and Werb, 2002; Barcellos-Hoff and Medina, 2005]. It is now recognized that a specific environment is necessary for the development and progression of tumors, and cancer may be a physiological response to an abnormal stromal environment [Barcellos-Hoff, 1998; Tlsty, 1998; Bissell and Radisky, 2001].

Nasopharyngeal carcinoma (NPC) is a human epithelial tumor with a high prevalence in the southern Chinese population and a high incidence of metastasis [Chang, 1992]. In addition to its rapid growth behavior, NPC has a great tendency to invade adjacent regions and metastasize to regional lymph node and distant organs. NPC is often locally advanced or already has spread to lymph nodes at time of diagnosis [Vokes et al., 1997]. Etiologic studies indicated that EBV infection, dietary exposure to carcinogens, and genetic susceptibility are associated with NPC [Raab-Traub, 2002; Xiong et al., 2004]. With the advances of molecular biology in the past decades, a lot of NPC-related molecules have been reported [Hui et al., 2005; Yau et al., 2006]. However, the molecular mechanism of NPC pathogenesis is still unclear. The stroma surrounding tumor cells actively interacts with the neoplastic cells, and regulates their behavior and malignant potential [Kalluri and Zeisberg, 2006]. NPC is also described as a lymphoepithelioma [Shanmugaratnam et al., 1979; Taxy et al., 1985] because of a characteristic heavy lymphoid infiltrate, indicating that the stroma, especially lymphoid infiltrate, may play an important role in NPC carcinogenesis. Using stroma as a sample may be an alterative way to study NPC carcinogenesis. Proteomics has been introduced as a new approach to cancer research and is currently considered to be a powerful tool for global evaluation of protein expression, providing new opportunities to screen for NPC stroma-related proteins. However, there has been no report of proteomic research on the NPC stroma.

Two-dimensional difference gel electrophoresis (2D-DIGE) is one of the approaches used for quantitative proteomics with great sensitivity and accuracy of quantitation. Using the 2D-DIGE approach, different samples pre-labeled with mass and charge matched fluorescent cyanine dyes are co-separated in the same 2-D gel, and an internal standard is used in every gel, overcoming the problem of intergel variation. In addition, this method reduces the number of gels needed for each experiment. Therefore, 2D-DIGE is able to efficiently provide the accurate and reproducible differential expression values for proteins in two or more biological samples [Friedman et al., 2004; Van den Bergh and Arckens, 2004; Kakisaka et al., 2007]. Proteomic analysis of clinical tissue samples may be the most direct and persuasive way to identify TS-related proteins. A major obstacle, however, to analyze tissue specimens is tissue heterogeneity. Laser capture microdissection (LCM) has been well established as a tool for purifying stromal cells from tissues, overcoming the problem of tissue heterogeneity and cell contamination.

To isolate NPC stroma-specific proteins, LCM was used to purify stromal cells from NPC and NNET, 2D-DIGE, and mass spectrometry (MS) were applied to identify the differential proteins in the NPC and normal stroma (NS), and the expression and location of two differential proteins (L-plastin and S100A9) were selectively confirmed by Western blotting and immunohistochemical analysis. To the best of our knowledge, it is the first time to analyze differential expression of proteins in tumor and NS by proteomic analysis. Our study may shed light on the role of NPC stromal cells and the interaction between NPC cells and their surrounding microenvironment.

MATERIALS AND METHODS

TISSUE COLLECTION

For 2D-DIGE and Western blotting, 42 fresh NPC tissues and 42 fresh normal nasopharyngeal epithelium tissues (NNET) from healthy individuals were obtained from the First Xiangya Hospital of Central South University, China at the time of diagnosis before any therapy with an informed consent. All samples were verified by histopathology before LCM. Among of these tissues, 30 cases were used for 2-D DIGE and 12 cases for Western blotting, respectively. Another group of formalin-fixed and paraffin-embedded tissues including 30 cases of NNET and 66 cases of primary NPC (54 males and 12 females, age 27–78 years, average 48 ± 9 years, TNM staging from II to IV) were obtained from the First Xiangya Hospital of Central South University, China, according to institutional regulations, and used for immunohistochemistry. According to the 1978 WHO classification [Shanmugaratnam and Sobin, 1993], 66 cases of primary NPC were histopathologically diagnosed as differentiated nonkeratinizing squamous cell carcinoma (WHO type II, moderately differentiated, 12 cases), and undifferentiated carcinoma (WHO type III, poorly differentiated, 54 cases).

LCM

LCM was performed with a Leica AS LMD system (Leica) as described previously [Cheng et al., 2008a]. Frozen sections (8 μm) from each NPC and NNET were prepared using a Leica CM 1900 cryostat (Leica) at -25°C. The sections were placed on a membrane-coated glass slides (Leica), fixed in 75% alcohol for 30 s, and stained with 0.5% violet-free methyl green (Sigma). The stained sections were air-dried and then subjected to LCM. Each cell population was determined to be 95% homogeneous by microscopic visualization of the captured cells (Fig. 1). As biopsy tissue specimens from one patient were too small to microdissect enough stromal cells for one time 2D-DIGE, pooled microdissected stromal cells from 10 NPC or NNET were used for each 2D-DIGE.

SAMPLE PREPARATION AND PROTEIN LABELING

After bleached with 70% chilled alcohol, the microdissected cells were dissolved in lysis buffer [30 mM Tris–Cl, 7 M urea, 2 M thiourea, 4% (w/v) CHAPS, pH 8.5, protease inhibitor cocktail] on ice for 1 h with sonicated intermittently, and then centrifuged at 12,000 rpm for 30 min at 4°C. The supernatant was collected and adjusted pH to 8.5 by 50 mM NaOH. The concentration of the total proteins was determined by 2-D Quantification kit (Amersham Biosciences). Equal amount proteins from all six sets samples were pooled together as the internal standard. The proteins were labeled with fluorescent cyanine dyes developed for 2D-DIGE (Amersham Biosciences) following the manufacturer's directions. The three NS sets and three TS sets were randomly labeled with Cy3 or Cy5, while

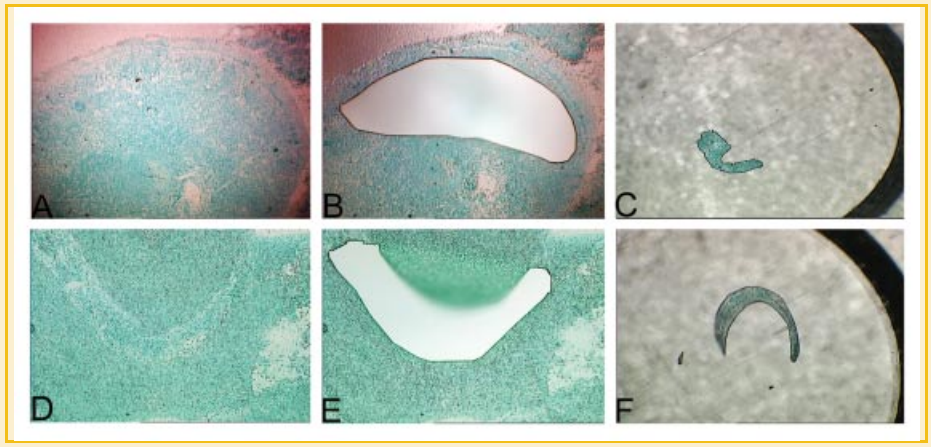

Fig. 1. LCM of tissues. NNET tissue before (A) and after (B) LCM, and captured normal stroma (C); NPC tissue before (D) and after (E) LCM, and captured tumor stroma (F).

internal standards were labeled with Cy2 using 400 pmol fluorochrome per 50 μg protein. Labeling reactions were conducted on ice in the dark for 30 min, and then quenched with 1 μl of 10 mM lysine (Sigma) for 10 min.

2D-DIGE

Fifty micrograms of Cy3- and Cy5-labeled samples from each set of NS group and TS group were combined before mixed with 50 μg Cy2-labeled internal standards. Equal volume of 2× sample buffer (8 M urea, 2 M thiourea, 4% CHAPS, 2% Bio-lyte, pH 4–7, 130 mM DTT) was added to the sample, and the total volume was made up to 450 μl with rehydration buffer (8 M urea, 4% CHAPS, 1% Bio-lyte, pH 4–7, 13 mM DTT). The proteins were applied to IPG strips (pH 4–7 NL, 24 cm) and focused on an IPGphor (Amersham Biosciences). Focused IPG strips were equilibrated, and then applied to 12% SDS polyacrylamide gels using low-fluorescence glass plates on Ettan DALT II system (Amersham Biosciences). All electrophoresis procedures were performed in the dark. The biological triplicate NS and TS sets and the internal standard were run on three gels as analytic gels. In addition, we performed another strip in parallel as a preparative gel for spots pickings as described in 2D-DIGE, except that the IPG strip was loaded with 1,000 μg proteins, and the gel was stained with Coomassie brilliant blue. After SDS–PAGE, the three analytic gels were scanned on the Typhoon 9410 scanner (GE Healthcare) at appropriate excitation/emission wavelengths specific for Cy2 (488/520 nm), Cy3 (532/580 nm), and Cy5 (633/670 nm) to generate nine protein spot maps.

IMAGING ANALYSIS

DeCyder 5.0 software (GE Healthcare) was used for 2D-DIGE analysis according to the manufacturer's recommendations. The DeCyder differential in-gel analysis (DIA) module was used for pair-wise comparisons of each NS and TS sample to the internal standard in each gel. The DeCyder biological variation analysis (BVA) module was then used to simultaneously match all nine protein-spot maps, and using the Cy3/Cy2 and Cy5/Cy2 DIA ratios calculate average abundance changes and paired Student's *t*-test *P*-values for the variance of these ratios for each protein pair across all samples. The differential protein spots ($|\text{ratio}|_{TS/NS} \geq 1.5$, $P \leq 0.05$) which were altered consistently in all nine protein-spot maps were selected for identification.

PROTEIN IDENTIFICATION BY MS

Protein spots of interest were excised from the preparative gel using punch, and in-gel trypsin digestion was performed as previously described [Yang et al., 2006]. The peptide was mixed with a CCA matrix solution. Mixture (1 μl) was analyzed with a Voyager System DE-STR 4307 MALDI-TOF Mass Spectrometer (MS) (ABI, Foster City, CA) to get a peptide mass fingerprint (PMF). In PMF, map database searching, MASCOT Distiller was used to obtain the monoisotopic peak list from the raw MS files. Peptide matching and protein searches against the NCBInr database were performed using the MASCOT search engine (http://www.matrixscience.com/) with a mass tolerance of ±50 ppm. Protein spots not identified or identified to be mixture by MALDI-TOF were subjected to analysis of ESI-Q-TOF MS (Micromass; Waters, Manchester, UK). Briefly, the samples were loaded on to a pre-column (320 μm × 50 mm, 5 μm C18 silica beads, Waters) at 30 μl/min flow rates for concentrations and fast desalting through a Waters CapLC autosampler, and then eluted to the reversed-phase column (75 μm × 150 mm, 5 μm, 100 Å, LC Packing) at a flow rate of 200 nl/min after flow splitting for separation. MS/MS spectra were performed in data-depended mode in which up to four precursor ions above an intensity threshold of 7 counts/seconds (cps) were selected for MS/MS analysis from each survey "scan." In MS/MS data database query, the peptide sequence tag (PKL) format file that generated from MS/MS was imported into the MASCOT search engine with an MS/MS tolerance of ±0.3 Da to search the NCBInr database.

WESTERN BLOTTING

Proteins from 12 pairs of microdissected stroma of fresh NPC and NNET were used for Western blotting as previously described by us [Yang et al., 2006]. Briefly, 40 μg of purified protein from each microdissected NS and TS were separated by 10% SDS–PAGE, and transferred to PVDF membrane (Bio-Rad). The blots were incubated for 2 h at room temperature in TBST (20 mM Tris–Cl, 140 mM NaCl,

pH 7.5, 0.05% Tween-20) containing 5% skim milk, and then were incubated with monoclonal mouse anti-L-plastin (dilution 1:800, Abcam) or monoclonal mouse anti-S100A9 (dilution 1:500, Santa Cruze Biotechnology) overnight at 4°C. After washing three times in TBST, membranes were incubated with a horseradish peroxidase-conjugated secondary antibody (dilution 1:2,000, Amersham Biosciences) for 1 h at room temperature. The blots were developed using ECL detection reagent, and quantitated by densitometry using ImageQuant image analysis system (Storm Optical Scanner). The mouse anti-β-actin (dilution 1:5,000, Sigma) was detected simultaneously as a loading control.

IMMUNOHISTOCHEMISTRY

Immunohistochemistry was done on paraffin-embedded specimens with anti-L-plastin (dilution 1:400) and anti-S100A9 (dilution 1:200) using the standard immunohistochemical technique. Briefly, paraffin sections (4 μm) were deparaffinized with xylene and rehydrated in a graded ethanol series, and treated with an antigen retrieval solution (10 mmol/L sodium citrate buffer, pH 6.0). Endogenous peroxidase activity was blocked with 3% hydrogen peroxide for 10 min at room temperature. Nonspecific binding was blocked with 1% normal serum in PBS for 10 min. The slides were incubated overnight at 4°C with either monoclonal mouse anti-L-plastin antibody (Abcam) or monoclonal mouse anti-s100A9 antibody (Santa Cruze Biotechnology), then were incubated with secondary antibody followed by avidin–biotin peroxidase complex (DAKO) according to the manufacturer's instructions. Finally, immunoreactivity was visualized using 3′, 3′-diaminobenzidine tetrachloride (DAB) (Sigma–Aldrich), and counterstained with hematoxylin. In negative controls, primary antibodies were replaced by PBS. Immunostaining was blindly evaluated by two independent experienced pathologists in an effort to provide a consensus on staining patterns. For L-plastin and S100A9, the numbers of positive cells per core were counted at a magnification of 40×.

STATISTICAL ANALYSIS

Statistical analysis was done using SPSS software (version 13.0). To evaluate the extent of S100A9 and L-plastin expression in NPC and NNET stroma, the number of positively stained cells in each specimen core was determined and the mean number of positive cells per duplicate patient core calculated. For the purpose of analysis, samples were categorized into two groups: those with S100A9-positive cell counts > median (high S100A9) and those with S100A9-positive cell counts ≤ median (low S100A9). Groups were similarly established for high and low L-plastin. Continuous variables were compared using the Mann–Whitney test. Significant differences between the expression of those two proteins and clinicopathologic factors, including age, gender, histologic type/grade (WHO), primary tumor (T) stage, and regional lymph node (N) metastasis were compared by the Mann–Whitney test or Kruskal–Wallis *H* test. Results were considered to be significant for *P*-values <0.05.

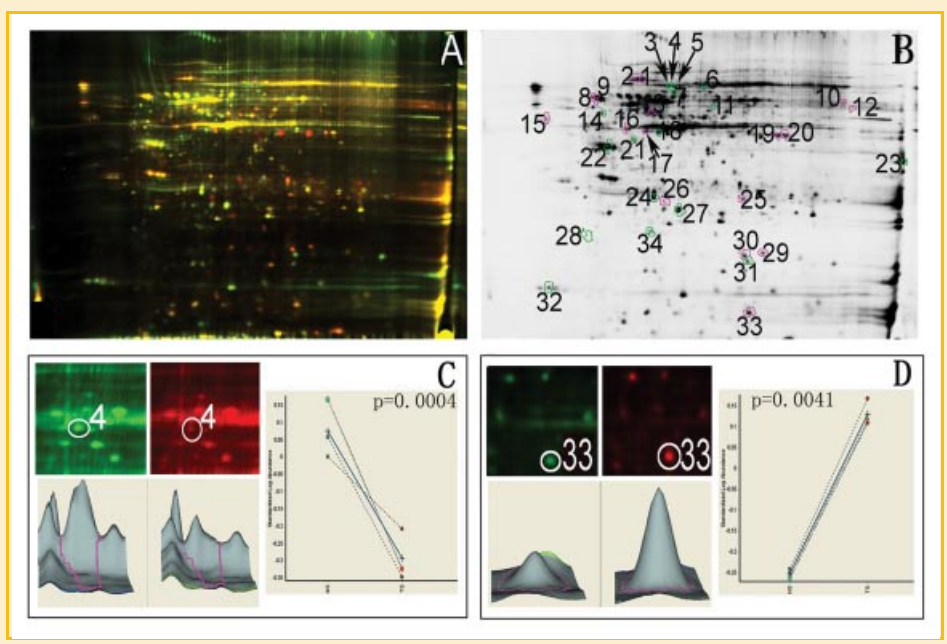

Fig. 2. Comparative proteomic analysis of the stroma of NPC and NNET tissue by 2D-DIGE. A: Representative two-color merged 2D-DIGE gel images of microdissected tumor and normal stroma. The proteins are labeled with either Cy3 (green, normal stroma) or Cy5 (red, tumor stroma) and subjected to 2D-DIGE using immobiline Dry IPG strips (pH 4–7). B: The differential protein spots detected by Decyder software, red circles indicate up-regulated proteins and blue circles indicate down-regulated proteins. C: Left top, a close-up of the region of 2D-DIGE gel images showing the significant down-expression of protein spot 4 in tumor stroma compared with normal stroma; left bottom, three-dimensional simulation of protein spot 4; right, the associated graph view of spot 4 indicated the average ratio of expression for spot 4, as obtained by computational analysis with DeCyder 5.0 software which allows the detection of significant abundance changes, *P*-value is 0.0004; D: left top, a close-up of the region of 2D-DIGE gel images showing the significant upexpression of protein spot 33 in tumor stroma compared with normal stroma; left bottom, three-dimensional simulation of protein spot 33; right, the associated graph view of spot 33, *P*-value is 0041.

RESULTS

DETECTION OF DIFFERENTIAL PROTEINS IN THE STROMA OF NPC AND NNET BY 2D-DIGE

Protein expression was compared between NPC and NS using 2D-DIGE with a mixed-sample internal standard. The interchangeable use of either Cy3 or Cy5 for either pooled set has already been established. After 2D-DIGE, the Cy2, Cy3, and Cy5 channels of each gel were individually imaged and the images were analyzed using DeCyder 5.0 software. Averages of $1{,}789 \pm 120$ protein spots were detected across all three 2D-DIGE gels. A two-color merged representative gel image is shown in Figure 2A (Cy3: NS, and Cy5: TS) indicating those proteins which expression levels changed consistently between the two biological samples. Thirty-four protein spots were differentially expressed ($|\text{ratio}|_{TS/NS} \geq 1.5$, $P < 0.05$) in all nine protein-spot maps (Fig. 2B). A close-up of the region of 2D-DIGE gel images, three-dimensional simulation, and the associated graph views of standardized log abundances of spots 4 and 33 were showed in Figure 2C,D. Spot 4 was significantly down-regulated ($P = 0.0004$) while spot 33 was significantly up-regulated ($P = 0.0041$) in TS compared with NS.

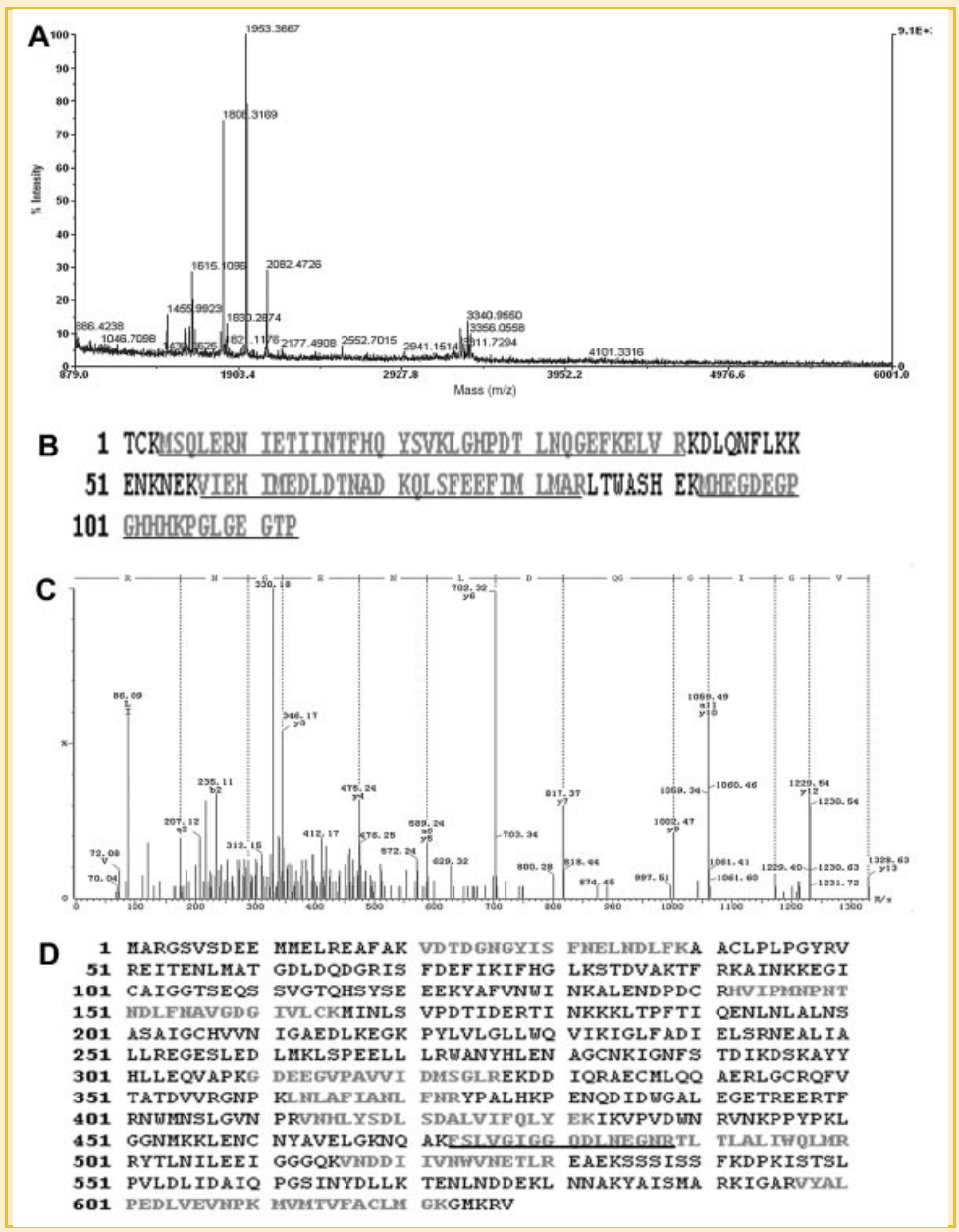

Fig. 3. MALDI-TOF MS and ESI-Q-TOF MS analysis of differential protein spots 33 and 4. A: MALDI-TOF MS mass spectrum of spot 33 identified as S100A9 according to the matched peaks was shown. B: Protein sequence of S100A9 was shown, and matched peptides were underlined. C: ESI-Q-TOF MS sequenced spectrum of spot 4, the amino acid sequence of a doubly charged peptide with m/z 801.4439 was identified as LVDQNIFSFYLSR from mass differences in the y-fragment ions series, and matched with residues 473–488 of L-plastin was shown. D: Protein sequence of L-plastin was shown, and matched peptides were underlined.

IDENTIFICATION OF DIFFERENTIAL PROTEINS BY MS

All of 34 differential protein spots were excised from the stained preparative gels, in situ digested with trypsin, and analyzed by MALDI-TOF MS and/or ESI-Q-TOF MS. A total of 20 differential proteins were identified. The MALDI-TOF MS map and database query result of a representative spot 33, and the ESI-Q-TOF MS map and database query result of a representative spot 4 are shown in Figure 3. A total of 30 monoisotopic peaks were input into MASCOT search engine to search the NCBInr database, and the query result showed that protein spot 33 was S100A9 (Fig. 3A,B). The MS/MS results of spot 4 are shown in Figure 3C,D. The amino acid sequence of a doubly charged peptide from spot 4 with m/z 838.3755 was identified as FSLVGIGGQDLNEGNR, which was a part of L-plastin sequence, and the query result indicated that protein spot 4 was L-plastin. The annotation of all the identified proteins is summarized in Table I. Proteins with higher abundance in TS compared to NS included periostin, s100A9, CapG, PYCARD, etc., while proteins with lower levels included L-plastin, Rho-GDI-β, B23, hnRNP K, etc. Based on the Human Protein Reference Database [Peri et al., 2003] (http://www.hprd.org/) recommendations, the 20 identified proteins are involved in signal transduction and cell communication, cell growth and/or maintenance, protein metabolism, energy pathways, transport, apoptosis, etc.

VALIDATION OF L-PLASTIN AND S100A9 EXPRESSION BY WESTERN BLOTTING

Western blotting was done to confirm differential expression of L-plastin and S100A9 in the 12 pairs of the microdissected stroma of NPC and NNET. Equal protein loading was proved by the parallel Western blotting of β-actin. As shown in Figure 4A,B, S100A9 was significantly up-regulated, whereas L-plastin was significantly down-regulated in the TS compared to NS ($P < 0.01$), which was consistent with the 2D-DIGE results and proved the credibility of 2D-DIGE analysis.

DETECTION OF THE EXPRESSION AND LOCATION OF L-PLASTIN AND S100A9 IN NPC AND NNET BY IMMUNOHISTOCHEMISTRY

To confirm the expression and location of L-plastin and S100A9, we further detected the expression of the two proteins using immunohistochemistry in 66 cases of primary NPC and 30 cases of NNET. Strong L-plastin immunostaining was readily detected in the lymphocyte cells of the NS (Fig. 5A1), whereas very weak staining was detectable in those of the TS (Fig. 5A2). Distinct S100A9 immunostaining was evident in inflammatory cells in the stromal component of all tumors (Fig. 5B2). Some tumors contained a limited number of S100A9-positive inflammatory cells (data not shown), while others displayed a high density of S100A9-positive

TABLE I. Differential Proteins Identified by MS After 2D-DIGE of the Tumor Stroma Versus Normal Stroma

Spot numbers[a]	Protein name	Accession no.	Mass	p*I*	MASCOT score	Method of identification	Sequence coverage (%)	Av. ratio[b]
1	BiP protein	gi|6470150	71,002	5.23	83	MALDI-TOF	68	1.71
2	GRP78 precursor	gi|386758	72,185	5.03	671	Both	71	1.59
3	L-plastin isoform 3	gi|114651523	70,815	5.2	355	ESI-Q-TOF MS	59	−1.56
	Heat shock 70 kDa protein 8 isoform 1	gi|5729877	71,082	5.37	139	ESI-Q-TOF MS	29	−1.56
4	L-plastin isoform 3	gi|114651523	70,815	5.2	390	ESI-Q-TOF MS	63	−2.34
5	Heat shock 70 kDa protein 8 isoform 1	gi|5729877	71,082	5.37	155	ESI-Q-TOF MS	29	−1.56
6	L-plastin variant	gi|62898171	70,785	5.2	203	ESI-Q-TOF MS	58	−2.02
7	Transformation up-regulated nuclear protein	gi|460789	51,325	5.13	377	ESI-Q-TOF MS	54	−1.52
8	Prolyl 4-hydroxylase	gi|20070125	57,480	4.76	639	ESI-Q-TOF MS	34	2.03
9	Prolyl 4-hydroxylase	gi|20070125	57,480	4.76	87	MALDI-TOF	34	2.03
10	Periostin, osteoblast specific factor	gi|5453834	93,901	7.57	93	MALDI-TOF	63	2.38
11	Not determined					Both		−2.74
12	Not determined					Both		1.81
13	Protein disulfide isomerase	gi|1710248	46,512	4.95	124	MALDI-TOF	33	1.81
14	Heterogeneous nuclear ribonucleoprotein H1	gi|5031753	49,484	5.89	146	MALDI-TOF	27	−2.59
15	Cytokeratin-1	gi|1346343	66,149	8.16	134	MALDI-TOF	25	1.55
16	Ribosomal protein SA, isoform CRA_c	gi|119584991	19,853	8.37	92	MALDI-TOF	55	1.66
17	Cytokeratin-1	gi|1346343	66,149	8.16	235	ESI-Q-TOF MS	25	1.55
18	Cytokeratin-19	gi|90111766	44,065	5.04	240	ESI-Q-TOF MS	21	−1.61
19	Gelsolin-like capping protein isoform 9	gi|55597035	38,779	5.88	72	MALDI-TOF	27	2.67
20	Gelsolin-like capping protein isoform 9	gi|55597035	38,779	5.88	80	MALDI-TOF	52	2.67
21	C protein	gi|306875	32,004	5.10	178	MALDI-TOF	53	−2.19
22	Nucleolar phosphoprotein B23	gi|190238	9,246	9.72	73	MALDI-TOF	17	−1.52
23	Heterogeneous nuclear ribonucleoprotein A2/B1	gi|73976124	32,524	8.74	67	MALDI-TOF	24	−1.61
24	Rho GDP dissociation inhibitor (GDI) beta	gi|56676393	23,031	5.10	202	MALDI-TOF	77	−2.61
25	PYCARD protein	gi|48257192	21,326	5.67	107	MALDI-TOF	43	1.93
26	Proapolipoprotein	gi|178775	28,944	5.45	176	MALDI-TOF	54	1.67
27	Chain A, crystal structure of lipid-free human apolipoprotein A-I	gi|90108664	28,061	5.27	85	MALDI-TOF	26	−1.63
28	Not determined					Both		−6.17
29	Nm23 protein	gi|35068	20,746	7.07	114	MALDI-TOF	25	1.99
30	Not determined					Both		2.42
31	Superoxide dismutase [Cu-Zn]	gi|31615344	16,154	5.7	98	MALDI-TOF	68	−1.89
32	Not determined					Both		−1.81
33	Mrp14 (migration inhibitory factor-related protein 14) (S100A9)	gi|20150229	13,159	5.71	106	MALDI-TOF	76	2.42
34	Not determined					Both		−1.51

[a]Spot numbers refer to those in Figure 2B.
[b]Av. ratio: tumor stroma/normal stroma.

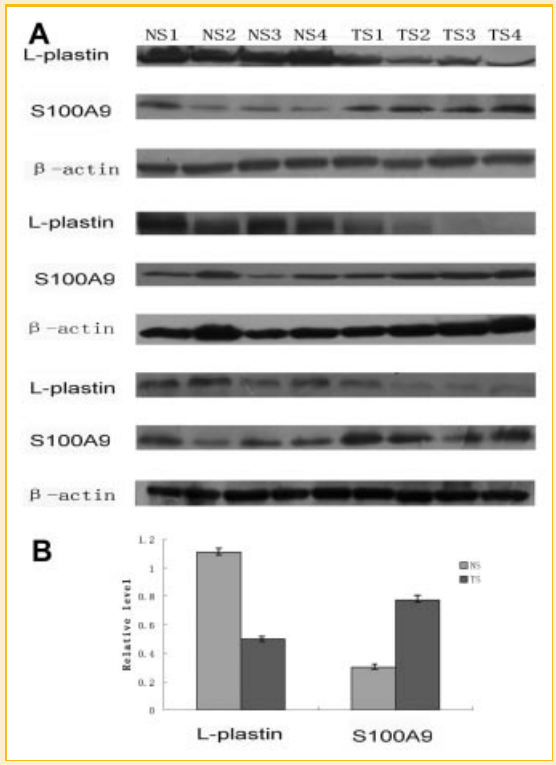

Fig. 4. Results of Western blotting of L-plastin and S100A9 in 12 pairs of microdissected stroma from NNET and NPC tissue. A: Western blotting shows changes in expression levels of L-plastin and S100A9 in tumor and normal stroma, β-actin is used as the internal loading control. B: Histogram shows the relative expression levels of L-plastin and S100A9 in 12 tumor stroma and 12 normal stroma as determined by densitometric analysis ($P = 0.002$).

cells infiltrating the tumor (Fig. 5B2). However, very weak staining was detectable in those of NS (Fig. 5B1). Additionally, the two proteins were not detected in the normal nasopharyngeal epithelial cells and cancer cells (Fig. 5). Statistical analysis indicated L-plastin significantly down-regulated in the TS versus NS, whereas S100A9 was significantly up-regulated in the TS versus NS (Table II, $P < 0.01$). The immunohistochemical result confirmed the different expression and stromal location of L-plastin and S100A9 in NPC and NNET. The correlation of several clinicopathologic factors with L-plastin and S100A9 expression status in 66 cases of primary NPC was shown in Table II. Tumors with the down-regulation of L-plastin tends to have a more advanced clinical stage and more poor differentiation (WHO III) ($P < 0.05$ or 0.01; Table II). In contrast, tumors with S100A9 up-regulation tends to have a more advanced clinical stage, more poor differentiation (WHO III) and regional lymph node metastasis ($P < 0.05$; Table II). The expression levels of both proteins did not correlate with the patients' age, gender, primary tumor stage, and regional lymph node metastasis.

DISCUSSION

Nasopharyngeal carcinoma is a disease with remarkable racial and geographic distribution, and it poses one of the most serious public health problems in southern China and Southeast Asia [Yu and Yuan, 2002]. The molecular mechanism of NPC pathogenesis remains to be elucidated. Our recent studies have identified certain proteins differentially expressed between normal nasopharyngeal epithelial and NPC cells, which might associate with the pathogenesis of NPC [Cheng et al., 2008a,b]. In current study, we screened for differentially expressed proteins in the stromal cells of normal human nasopharyngeal and NPC tissue by 2D-DIGE and MS. As a result, 20 differential proteins were successfully identified in tumor and NS, which are involved in a variety of biological processes, such as signal transduction and cell communication, energy metabolism, protein metabolism, cell growth and/or maintenance, immune response, transport, and apoptosis (Table I). The clinicopathological analysis by immunohistochemistry was performed to detect expression of the two proteins in NPC and NNET tissue specimens. The data showed that expression levels of the two proteins were significantly correlated with clinical stage and differentiation of NPC.

Plastins belong to the family of actin-binding proteins which exhibit a tissue-specific expression pattern. In mammals, there are three plastin isoforms: T-plastin is expressed in the cells derived from solid tissue, I-plastin is specifically expressed in the microvilli of the small intestine and the kidney, and L-plastin expression is found in the hematopoietic cell lineage. L-plastin has been proposed to be involved in the control of cell adhesion and motility. A number of experiments performed with macrophages and polymorphonuclear neutrophils (PMN) suggested a role for L-plastin in regulating integrin-mediated adhesion [Wang et al., 2001]. Several studies found that L-plastin could be detected in normal myoepithelial cells of the mammary gland [Zheng et al., 1997; Lapillonne et al., 2000]. In the present study, L-plastin was down-regulated in the TS versus NS, highly expressed in the lymphocyte cells of the NS. Although it is not yet fully elucidated, the role of L-plastin in cancer-associated stroma is certainly an interesting issue due to the highlighted significance of tumor–stromal interactions by recent reports [Kenny and Bissell, 2003; Mueller and Fusenig, 2004]. Our study indicates the complex interaction between NPC cells and the surrounding host tissue possibly through L-plastin.

S100A9 protein, a calcium-binding protein, was originally discovered as an immunogenic protein expressed and secreted by neutrophils [Arai et al., 1999; Donato, 1999; Heizmann et al., 2002]. It regulated various calcium-mediated cellular functions such as cell growth, differentiation, migration, and signal transduction, and was associated with neoplastic disorders [Arai et al., 2004]. Subsequently, it emerged as an important proinflammatory mediator in acute and chronic inflammation [Gebhardt et al., 2006]. The protein had been implicated in a variety of chronic inflammatory conditions such as cystic fibrosis, rheumatoid arthritis, tuberculosis, and transplant rejection [Odink et al., 1987; Nacken et al., 2003]. S100A9 often formed a stable heterodimer complex with S100A8 (S100A8/A9) at sites of inflammation [Nacken et al., 2003] and were highly chemotactic, contributing to host inflammatory responses such as leukocyte trafficking, adhesion, and migration [Nacken et al., 2003; Ryckman et al., 2004]. S100A9 is overexpressed in many human tumors and specifically involved in tumor development or progression [Grote et al., 2006;

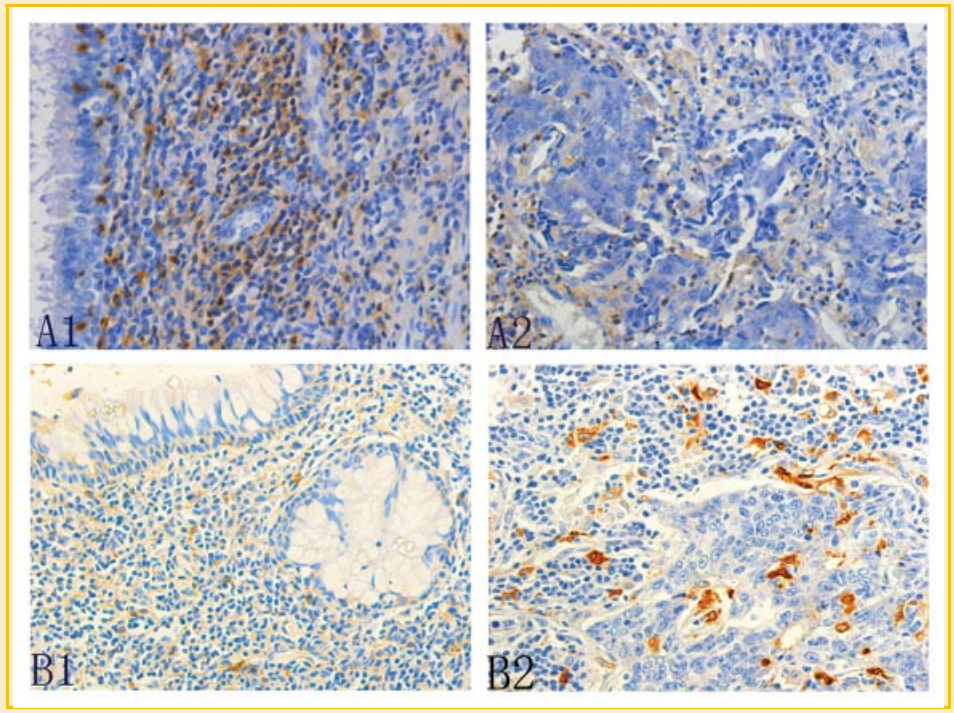

Fig. 5. Representative photographs of immunohistochemistry of L-plastin and S100A9 in the NNET and NPC specimens. A: Immunohistochemistry of L-plastin, strong staining in the stroma of NNET (1), weak staining in the stroma of primary NPC (2), no staining was detectable in the nasopharyngeal epithelial cells and cancer cells; B: Immunohistochemistry of S100A9, weak staining in the stroma of NNET (1), strong staining in the stroma of primary NPC (2), it was not detected in the nasopharyngeal epithelial cells and cancer cells. Original magnification, 400×.

TABLE II. Relationships Between L-plastin, S100A9 Expression, and Clinicopathologic Factors in NPC

		L-plastin			S100A9		
Variables	n	Low	High	*P*	Low	High	*P*
Group				0.000*			0.000*
NNET	30	7	23		25	5	
NPC	66	57	9		15	51	
Age				0.435			0.271
≤50	31	27	4		6	25	
50	35	30	5		9	26	
Gender				0.278			0.168
Male	54	46	8		11	43	
Female	12	11	1		4	8	
Histology type (WHO)				0.015*			0.0005*
WHO II	12	8	4		7	5	
WHO III	54	49	5		8	46	
Primary tumor (T) stage				0.430			0.449
T1	18	16	2		3	15	
T2	23	19	4		6	17	
T3	20	18	2		5	15	
T4	5	4	1		1	4	
Regional lymph node (N) metastasis				0.233			0.011*
N0	7	5	2		4	3	
N1	11	8	3		5	6	
N2	31	28	3		3	28	
N3	17	16	1		3	14	
Clinical stage				0.000*			0.005*
II	7	2	5		5	2	
III	38	36	2		6	32	
IV	21	19	2		4	17	

*$P < 0.05$ or 0.01 by Mann–Whitney test or Kruskal–Wallis H test.

Sheikh et al., 2007]. Hiratsuka et al. [2006] showed that the expression of S100A8/S100A9 was induced in the lungs of mice with distant primary tumors. This in turn attracted myeloid cells to the lungs and ultimately supported the invasion of tumor cells to this site. Their result further showed that factors such as vascular endothelial growth factor-A and transforming growth factor-beta (TGF-β) induced the expression of S100A9 and supported a role for the protein in the pre-metastatic phase of cancer dissemination. Sheikh et al., [2007] reported that the monocytes/immature macrophages (i.e., $CD141/CD68^{-}$) were strongly positive for S100A9, while strongly positive neutrophils were also observed in blood vessels around the tumor. In our study, S100A9 was up-regulated in the stromal myeloid cells, and monocytes/macrophages of NPC, suggesting that S100A9 might contribute to the host inflammation responses to the tumor.

Periostin, one of the up-regulated in the NPC stroma, was frequently observed in the stroma of breast cancer and pancreatic adenocarcinoma, and was related to cancer invasion and metastasis by regulating signal transduction and cell communication [Grigoriadis et al., 2006; Kudo et al., 2007; Kanno et al., 2008]. CapG (macrophage capping protein) is another up-regulated protein in the NPC stroma and a member of the actin-binding of protein family. CapG is involved in cell growth and/or maintenance through regulating cell motility [Witke et al., 2001; Parikh et al., 2003]. Down-regulated proteins in NPC stroma, such as heterogeneous nuclear ribonucleoproteins C1/C2, heterogeneous nuclear ribonucleoprotein A2/B1, transformation up-regulated nuclear protein, and heterogeneous nuclear ribonucleoprotein H1 were involved in

regulation of cleobase, nucleoside, and nucleic acid metabolism [Celis et al., 2005]. Even though some of these differential stromal proteins were investigated in NPC, the potential role of these proteins involved in the development of NPC deserves further exploration.

In summary, our data have demonstrated the feasibility of using a proteomic strategy coupled with LCM to identify stromal proteins associated with NPC carcinogenesis. Our findings are an initial step toward studying the role of stroma in the NPC carcinogenesis, as well as the interaction between NPC cells and their surrounding microenvironment. However, great efforts will be required to elucidate the functional roles of the stromal proteins in NPC.

ACKNOWLEDGMENTS

National Key Basic Research Program of China, Outstanding Scholars of New Era from Ministry of Education of China, Hibiscus Scholars of Hunan Province, China, key research program from Science and Technology Committee of Hunan, China, key research program from Public Health Bureau of Hunan Province, China, grants from National Natural Sciences Foundation of China, Program for New Century Excellent Talents in University (NCET); grant numbers: 2001CB510207, 2002-48, 2007-362, 04XK1001-1, 05SK1004-1, Z02-04, 30500558, 30670990, 2007-70.

REFERENCES

Arai K, Mizuno K, Yamada T, Nozawa R. 1999. Immunohistochemical evaluation of MRP-14 expression in epithelioid granuloma using monoclonal antibody 60B8. J Investig Allergol Clin Immunol 9:21–26.

Arai K, Teratani T, Kuruto-Niwa R, Yamada T, Nozawa R. 2004. S100A9 expression in invasive ductal carcinoma of the breast: S100A9 expression in adenocarcinoma is closely associated with poor tumour differentiation. Eur J Cancer 40:1179–1187.

Barcellos-Hoff MH. 1998. The potential influence of radiation-induced microenvironments in neoplastic progressioneditor editors. J Mammary Gland Biol Neoplasia 3:165–175.

Barcellos-Hoff MH, Medina D. 2005. New highlights on stroma-epithelial interactions in breast cancer. Breast Cancer Res 7:33–336.

Bingle L, Brown NJ, Lewis CE. 2002. The role of tumour-associated macrophages in tumour progression: Implications for new anticancer therapies. J Pathol 196:254–265.

Bissell MJ, Radisky D. 2001. Putting tumours in context. Nat Rev Cancer 1: 46–54.

Celis JE, Moreira JM, Cabezon T, Gromov P, Friis E, Rank F, Gromova I. 2005. Identification of extracellular and intracellular signaling components of the mammary adipose tissue and its interstitial fluid in high risk breast cancer patients: Toward dissecting the molecular circuitry of epithelial-adipocyte stromal cell interactions. Mol Cell Proteomics 4:492–522.

Chang YL. 1992. Nasopharyngeal carcinoma in Taiwan. J Formos Med Assoc 91:S8–S18.

Cheng AL, Huang WG, Chen ZC, Peng F, Zhang PF, Li MY, Li F, Li JL, Li C, Yi H, Yi B, Xiao ZQ. 2008a. Identification of novel nasopharyngeal carcinoma biomarkers by laser capture microdissection and proteomic analysis. Clin Cancer Res 14:435–445.

Cheng AL, Huang WG, Chen ZC, Zhang PF, Li MY, Li F, Li JL, Li C, Yi H, Peng F, Duan CJ, Xiao ZQ. 2008b. Identificating cathepsin D as a biomarker for differentiation and prognosis of nasopharyngeal carcinoma by laser capture microdissection and proteomic analysis. J Proteome Res 7:2415–2426.

Coussens LM, Werb Z. 2001. Inflammatory cells and cancer: Think different. J Exp Med 193:F23–F26.

Cruz-Munoz W, Kim I, Khokha R. 2006. TIMP-3 deficiency in the host, but not in the tumor, enhances tumor growth and angiogenesis. Oncogene 25: 650–655.

Donato R. 1999. Functional roles of S100 proteins, calcium-binding proteins of the EF-hand type. Biochim Biophys Acta 1450:191–231.

Fidler IJ. 2001. Angiogenic heterogeneity: Regulation of neoplastic angiogenesis by the organ microenvironment. J Natl Cancer Inst 93:1040–1041.

Friedman DB, Hill S, Keller JW, Merchant NB, Levy SE, Coffey RJ, Caprioli RM. 2004. Proteome analysis of human colon cancer by two-dimensional difference gel electrophoresis and mass spectrometry. Proteomics 4:793–811.

Gebhardt C, Nemeth J, Angel P, Hess J. 2006. S100A8 and S100A9 in inflammation and cancer. Biochem Pharmacol 72:1622–1631.

Grigoriadis A, Mackay A, Reis-Filho JS, Steele D, Iseli C, Stevenson BJ, Jongeneel CV, Valgeirsson H, Fenwick K, Iravani M, Leao M, Simpson AJ, Strausberg RL, Jat PS, Ashworth A, Neville AM, O'Hare MJ. 2006. Establishment of the epithelial-specific transcriptome of normal and malignant human breast cells based on MPSS and array expression data. Breast Cancer Res 8:R56.

Grote J, Konig S, Ackermann D, Sopalla C, Benedyk M, Los M, Kerkhoff C. 2006. Identification of poly(ADP-ribose)polymerase-1 and Ku70/Ku80 as transcriptional regulators of S100A9 gene expression. BMC Mol Biol 7:48.

Heizmann CW, Fritz G, Schafer BW. 2002. S100 proteins: Structure, functions and pathology. Front Biosci 7:d1356–d1368.

Hiratsuka S, Watanabe A, Aburatani H, Maru Y. 2006. Tumour-mediated upregulation of chemoattractants and recruitment of myeloid cells predetermines lung metastasis. Nat Cell Biol 8:1369–1375.

Hui AB, Or YY, Takano H, Tsang RK, To KF, Guan XY, Sham JS, Hung KW, Lam CN, van Hasselt CA, Kuo WL, Gray JW, Huang DP, Lo KW. 2005. Array-based comparative genomic hybridization analysis identified cyclin D1 as a target oncogene at 11q13.3 in nasopharyngeal carcinoma. Cancer Res 65:8125–8133.

Kakisaka T, Kondo T, Okano T, Fujii K, Honda K, Endo M, Tsuchida A, Aoki T, Itoi T, Moriyasu F, Yamada T, Kato H, Nishimura T, Todo S, Hirohashi S. 2007. Plasma proteomics of pancreatic cancer patients by multi-dimensional liquid chromatography and two-dimensional difference gel electrophoresis (2D-DIGE): Up-regulation of leucine-rich alpha-2-glycoprotein in pancreatic cancer. J Chromatogr B Analyt Technol Biomed Life Sci 852:257–267.

Kalluri R, Zeisberg M. 2006. Fibroblasts in cancer. Nat Rev Cancer 6:392–401.

Kanno A, Satoh K, Masamune A, Hirota M, Kimura K, Umino J, Hamada S, Satoh A, Egawa S, Motoi F, Unno M, Shimosegawa T. 2008. Periostin, secreted from stromal cells, has biphasic effect on cell migration and correlates with the epithelial to mesenchymal transition of human pancreatic cancer cells. Int J Cancer 122:2707–2718.

Kenny PA, Bissell MJ. 2003. Tumor reversion: Correction of malignant behavior by microenvironmental cues. Int J Cancer 107:688–695.

Koukourakis MI, Giatromanolaki A, Brekken RA, Sivridis E, Gatter KC, Harris AL, Sage EH. 2003. Enhanced expression of SPARC/osteonectin in the tumor-associated stroma of non-small cell lung cancer is correlated with markers of hypoxia/acidity and with poor prognosis of patients. Cancer Res 63:5376–5380.

Kudo Y, Siriwardena BS, Hatano H, Ogawa I, Takata T. 2007. Periostin: Novel diagnostic and therapeutic target for cancer. Histol Histopathol 22:1167–1174.

Lapillonne A, Coue O, Friederich E, Nicolas A, Del Maestro L, Louvard D, Robine S, Sastre-Garau X. 2000. Expression patterns of L-plastin isoform in normal and carcinomatous breast tissues. Anticancer Res 20:3177–3182.

Liotta LA, Kohn EC. 2001. The microenvironment of the tumour-host interface. Nature 411:375–379.

Mueller MM, Fusenig NE. 2004. Friends or foes—Bipolar effects of the tumour stroma in cancer. Nat Rev Cancer 4:839–849.

Muerkoster S, Wegehenkel K, Arlt A, Witt M, Sipos B, Kruse ML, Sebens T, Kloppel G, Kalthoff H, Folsch UR, Schafer H. 2004. Tumor stroma interactions induce chemoresistance in pancreatic ductal carcinoma cells involving increased secretion and paracrine effects of nitric oxide and interleukin-1beta. Cancer Res 64:1331–1337.

Nacken W, Roth J, Sorg C, Kerkhoff C. 2003. S100A9/S10A8: Myeloid representatives of the S100 protei family as prominent players in innate immunity. Microsc Res Tech 60:569–580.

Odink K, Cerletti N, Bruggen J, Clerc RG, Tarcsay L, Zwadlo G, Gerhards G, Schlegel R, Sorg C. 1987. Two calcium-binding proteins in infiltrate macrophages of rheumatoid arthritis. Nature 330:80–82.

Ohuchida K, Mizumoto K, Murakami M, Qian LW, Sato N, Nagai E, Matsumoto K, Nakamura T, Tanaka M. 2004. Radiation to stromal fibroblasts increases invasiveness of pancreatic cancer cells through tumor-stromal interactions. Cancer Res 64:3215–3222.

Olumi AF, Grossfeld GD, Hayward SW, Carroll PR, Tlsty TD, Cunha GR. 1999. Carcinoma-associated fibroblasts direct tumor progression of initiated human prostatic epithelium. Cancer Res 59:5002–5011.

Parikh SS, Litherland SA, Clare-Salzler MJ, Li W, Gulig PA, Southwick FS. 2003. CapG(−/−) mice have specific host defense defects that render them more susceptible than CapG(+/+) mice to Listeria monocytogenes infection but not to Salmonella enterica serovar Typhimurium infection. Infect Immun 71:6582–6590.

Peri S, Navarro JD, Amanchy R, Kristiansen TZ, Jonnalagadda CK, Surendranath V, Niranjan V, Muthusamy B, Gandhi TK, Gronborg M, Ibarrola N, Deshpande N, Shanker K, Shivashankar HN, Rashmi BP, Ramya MA, Zhao Z, Chandrika KN, Padma N, Harsha HC, Yatish AJ, Kavitha MP, Menezes M, Choudhury DR, Suresh S, Ghosh N, Saravana R, Chandran S, Krishna S, Joy M, Anand SK, Madavan V, Joseph A, Wong GW, Schiemann WP, Constantinescu SN, Huang L, Khosravi-Far R, Steen H, Tewari M, Ghaffari S, Blobe GC, Dang CV, Garcia JG, Pevsner J, Jensen ON, Roepstorff P, Deshpande KS, Chinnaiyan AM, Hamosh A, Chakravarti A, Pandey A. 2003. Development of human protein reference database as an initial platform for approaching systems biology in humans. Genome Res 13:2363–2371.

Raab-Traub N. 2002. Epstein-Barr virus in the pathogenesis of NPC. Semin Cancer Biol 12:431–441.

Ryckman C, Gilbert C, de Medicis R, Lussier A, Vandal K, Tessier PA. 2004. Monosodium urate monohydrate crystals induce the release of the proinflammatory protein S100A8/A9 from neutrophils. J Leukoc Biol 76:433–440.

Shanmugaratnam K, Sobin LH. 1993. The World Health Organization histological classification of tumours of the upper respiratory tract and ear. A. commentary on the second edition. Cancer 71:2689–2697.

Shanmugaratnam K, Chan SH, de-The G, Goh JE, Khor TH, Simons MJ, Tye CY. 1979. Histopathology of nasopharyngeal carcinoma: Correlations with epidemiology, survival rates and other biological characteristics. Cancer 44:1029–1044.

Sheikh AA, Vimalachandran D, Thompson CC, Jenkins RE, Nedjadi T, Shekouh A, Campbell F, Dodson A, Prime W, Crnogorac-Jurcevic T, Lemoine NR, Costello E. 2007. The expression of S100A8 in pancreatic cancer-associated monocytes is associated with the Smad4 status of pancreatic cancer cells. Proteomics 7:1929–1940.

Silberstein GB. 2001. Tumour-stromal interactions. Role of the stroma in mammary development. Breast Cancer Res 3:218–223.

Taxy JB, Hidvegi DF, Battifora H. 1985. Nasopharyngeal carcinoma: Anti-keratin immunohistochemistry and electron microscopy. Am J Clin Pathol 83:320–325.

Tlsty TD. 1998. Cell-adhesion-dependent influences on genomic instability and carcinogenesis. Curr Opin Cell Biol 10:647–653.

Van den Bergh G, Arckens L. 2004. Fluorescent two-dimensional difference gel electrophoresis unveils the potential of gel-based proteomics. Curr Opin Biotechnol 15:38–43.

Vokes EE, Liebowitz DN, Weichselbaum RR. 1997. Nasopharyngeal carcinoma. Lancet 350:1087–1091.

Wang J, Chen H, Brown EJ. 2001. L-plastin peptide activation of alpha(v)-beta(3)-mediated adhesion requires integrin conformational change and actin filament disassembly. J Biol Chem 276:14474–14481.

Wernert N. 1997. The multiple roles of tumour stroma. Virchows Arch 430:433–443.

Wernert N, Locherbach C, Wellmann A, Behrens P, Hugel A. 2001. Presence of genetic alterations in microdissected stroma of human colon and breast cancers. Anticancer Res 21:2259–2264.

Wiseman BS, Werb Z. 2002. Stromal effects on mammary gland development and breast cancer. Science 296:1046–1049.

Witke W, Li W, Kwiatkowski DJ, Southwick FS. 2001. Comparisons of CapG and gelsolin-null macrophages: Demonstration of a unique role for CapG in receptor-mediated ruffling, phagocytosis, and vesicle rocketing. J Cell Biol 154:775–784.

Xiong W, Zeng ZY, Xia JH, Xia K, Shen SR, Li XL, Hu DX, Tan C, Xiang JJ, Zhou J, Deng H, Fan SQ, Li WF, Wang R, Zhou M, Zhu SG, Lu HB, Qian J, Zhang BC, Wang JR, Ma J, Xiao BY, Huang H, Zhang QH, Zhou YH, Luo XM, Zhou HD, Yang YX, Dai HP, Feng GY, Pan Q, Wu LQ, He L, Li GY. 2004. A susceptibility locus at chromosome 3p21 linked to familial nasopharyngeal carcinoma. Cancer Res 64:1972–1974.

Yang YX, Xiao ZQ, Chen ZC, Zhang GY, Yi H, Zhang PF, Li JL, Zhu G. 2006. Proteome analysis of multidrug resistance in vincristine-resistant human gastric cancer cell line SGC7901/VCR. Proteomics 6:2009–2021.

Yau WL, Lung HL, Zabarovsky ER, Lerman MI, Sham JS, Chua DT, Tsao SW, Stanbridge EJ, Lung ML. 2006. Functional studies of the chromosome 3p21.3 candidate tumor suppressor gene BLU/ZMYND10 in nasopharyngeal carcinoma. Int J Cancer 119:2821–2826.

Yu MC, Yuan JM. 2002. Epidemiology of nasopharyngeal carcinoma. Semin Cancer Biol 12:421–429.

Zheng J, Rudra-Ganguly N, Miller GJ, Moffatt KA, Cote RJ, Roy-Burman P. 1997. Steroid hormone induction and expression patterns of L-plastin in normal and carcinomatous prostate tissues. Am J Pathol 150:2009–2018.